Monoubiquitin-dependent endocytosis of the IRON-REGULATED TRANSPORTER 1 (IRT1) transporter controls iron uptake in plants

Marie Barberon[a,1], Enric Zelazny[a,1], Stéphanie Robert[b,c,d], Geneviève Conéjéro[a], Cathy Curie[a], Jiří Friml[b,c], and Grégory Vert[a,2]

[a]Biochimie et Physiologie Moléculaire des Plantes, Centre National de la Recherche Scientifique Unité Mixte de Recherche 5004, Institut de Biologie Intégrative des Plantes, 34060 Montpellier Cedex 2, France; [b]Department of Plant Systems Biology, Flanders Interuniversity Institute of Biotechnology, 9052 Ghent, Belgium; [c]Departments of Plant Biotechnology and Genetics, University of Ghent, 9052 Ghent, Belgium; and [d]Departments of Forest Genetics and Plant Physiology, Swedish University of Agricultural Sciences/Umea Plant Science Center, 901 83 Umea, Sweden

Edited* by Joanne Chory, Salk Institute for Biological Studies and Howard Hughes Medical Institute, La Jolla, CA, and approved May 11, 2011 (received for review January 13, 2011)

Plants take up iron from the soil using the IRON-REGULATED TRANSPORTER 1 (IRT1) high-affinity iron transporter at the root surface. Sophisticated regulatory mechanisms allow plants to tightly control the levels of IRT1, ensuring optimal absorption of essential but toxic iron. Here, we demonstrate that overexpression of *Arabidopsis thaliana* IRT1 leads to constitutive IRT1 protein accumulation, metal overload, and oxidative stress. IRT1 is unexpectedly found in *trans*-Golgi network/early endosomes of root hair cells, and its levels and localization are unaffected by iron nutrition. Using pharmacological approaches, we show that IRT1 cycles to the plasma membrane to perform iron and metal uptake at the cell surface and is sent to the vacuole for proper turnover. We also prove that IRT1 is monoubiquitinated on several cytosol-exposed residues in vivo and that mutation of two putative monoubiquitination target residues in IRT1 triggers stabilization at the plasma membrane and leads to extreme lethality. Together, these data suggest a model in which monoubiquitin-dependent internalization/sorting and turnover keep the plasma membrane pool of IRT1 low to ensure proper iron uptake and to prevent metal toxicity. More generally, our work demonstrates the existence of monoubiquitin-dependent trafficking to lytic vacuoles in plants and points to proteasome-independent turnover of plasma membrane proteins.

ubiquitin | protein dynamic | plant cell biology

Iron is an essential nutrient for virtually all organisms because it plays critical roles in life-sustaining processes. Iron's facile ability to gain and lose electrons has made it a cofactor for enzymes involved in a wide variety of oxidation-reduction reactions, such as photosynthesis, respiration, hormone synthesis, and DNA synthesis (1). This essential role of iron is evidenced by the disorders that its deficiency promotes, including severe anemia in mammals or chlorosis in plants (2). Despite its absolute requirement, iron reacts in cells with oxygen and generates noxious reactive oxygen species that are deleterious for plant growth and development (1). Cellular and whole-organism iron homeostasis must therefore be strictly balanced. Although abundant in nature, iron is often available in limited amounts because it is mostly present in rather insoluble Fe(III) complexes in soils. The IRON-REGULATED TRANSPORTER 1 (IRT1) root iron transporter from the model plant *Arabidopsis* takes up iron, as well as other metals, from the soil upon iron deficiency (3). IRT1 is a major player in the regulation of plant iron homeostasis, as attested by the severe chlorosis and lethality of an *irt1-1* knockout mutant (3, 4). Consistently, the *IRT1* gene is highly expressed in iron-starved root peripheral cell layers, namely, the epidermis and the underlying cortex (3). The resultant IRT1-dependent iron absorption allows proper growth and development under iron-limited conditions (3, 4).

Recently, some of the molecular mechanisms that control *IRT1* expression and iron homeostasis have been uncovered. Iron deficiency transcriptionally promotes strong *IRT1* gene expression in root peripheral cell layers via the bHLH transcription factor Fe–DEFICIENCY-INDUCED TRANSCRIPTION FACTOR (FIT), a positive regulator of root iron deficiency responses (5–7). In parallel, constitutive expression of *IRT1* revealed post-transcriptional control of *IRT1*, with iron sufficiency triggering a decrease in IRT1 protein levels in roots (8). FIT was also proposed to act posttranscriptionally on *IRT1* by promoting IRT1 protein accumulation in iron-deficient roots (5). Although the exact molecular mechanisms underlying such posttranscriptional regulations are unclear, IRT1 was suggested to be regulated at the protein stability level by iron (5, 8).

Ubiquitination is well known in yeast and metazoans to mediate internalization of plasma membrane proteins, such as receptors and transporters, as well as their sorting into later endosomal compartments on their way to the vacuole/lysosome for degradation (9). In particular, monoubiquitination was shown to be sufficient for endocytosis of the Ste2p yeast α-factor receptor and the EGF receptor (EGFR) in mammals (10, 11). As such, ubiquitination is involved in a diverse array of cellular processes, including nutrient uptake; morphogenesis of the neuronal network; synaptic molecule recycling; and regulation of the cell-surface receptors, transporters, and channels (12). So far, there is only little evidence about ubiquitination of plasma membrane proteins in plants. Only the auxin efflux carrier PIN2, the water channel aquaporin PIP2;1, and the flagellin receptor FLS2 were experimentally shown to be ubiquitinated in vivo (13–15). In these three examples, ubiquitination was, however, proposed to be associated with proteasome-dependent degradation since the 26S proteasome inhibitor MG132 led to overaccumulation of the corresponding proteins (13–15).

To shed light on the molecular mechanisms driving the degradation of plasma membrane proteins and the poorly documented ubiquitin-dependent endocytosis in plants, we characterized further *IRT1* posttranscriptional control. To this purpose, we thoroughly investigated the levels, turnover rate, localization, and dynamics of endogenous and constitutively expressed IRT1

Author contributions: M.B., E.Z., and G.V. designed research; M.B., E.Z., and S.R. performed research; S.R., G.C., and J.F. contributed new reagents/analytic tools; M.B., E.Z., C.C., and G.V. analyzed data; and M.B., E.Z., and G.V. wrote the paper.

The authors declare no conflict of interest.

*This Direct Submission article had a prearranged editor.

[1]M.B. and E.Z. contributed equally to this work.

[2]To whom correspondence should be addressed. E-mail: gregory.vert@supagro.inra.fr.

See Author Summary on page 12985.

This article contains supporting information online at www.pnas.org/lookup/suppl/doi:10.1073/pnas.1100659108/-/DCSupplemental.

protein in root epidermal cells. We found that IRT1 protein localizes to early endosomal compartments but cycles with the plasma membrane and traffics to the vacuole for constant turnover. We also demonstrate that monoubiquitination of IRT1 controls its trafficking from the plasma membrane and targeting to the vacuole. Expression in transgenic plants of a mutant version of IRT1 defective in ubiquitination leads to increased IRT1 levels at the plasma membrane and extreme lethality, highlighting the necessity for tight control of IRT1 localization. Taken together, our results establish a crucial role for monoubiquitination in iron uptake as well as plant growth and development and more generally demonstrate the existence of monoubiquitin-dependent trafficking and turnover of membrane proteins in plants.

Results

IRT1 Is Not Subjected to an Iron-Dependent Degradation. To grasp the molecular mechanisms driving endocytosis in plants, we reinvestigated *IRT1* iron-dependent posttranscriptional regulation by monitoring IRT1 protein accumulation and turnover in response to changes in iron nutrition. To circumvent the strong transcriptional regulation of *IRT1* by iron, we generated transgenic plants expressing full-length *IRT1* cDNA under the control of the constitutive *CaMV35S* promoter in the *irt1-1* mutant background, where no endogenous IRT1 is found (3). Expression of 35S::IRT1 complemented both the chlorosis and metal accumulation defect of *irt1-1* in iron-limited conditions (Figs. 1*A* and 2) and led to constitutive *IRT1* mRNA accumulation in roots (Fig. 1*B*) and leaves (Fig. 1*C*). Western blot analyses on several independent transgenic lines indicated that IRT1 protein expressed from the transgene accumulated irrespective of the iron supply in both roots (Fig. 1*D*) and leaves (Fig. 1*E*), where endogenous IRT1 is absent or barely detected in WT plants.

Because these results contrast with those of previous reports suggesting an iron-dependent destabilization of IRT1 (8), we determined the half-life of endogenous IRT1 protein in the presence of the translation inhibitor cycloheximide (CHX). Total IRT1 protein levels decayed to reach basal level at 24 h, regardless of iron supply to the roots (Fig. 1*F*). The half-life of IRT1 protein was estimated to be ~5 h under the two iron regimes (Fig. S1). To validate our observations further, we then revisited the hypothesis that FIT acts posttranscriptionally on *IRT1* to promote IRT1 protein accumulation under iron starvation (5). In our hands, *fit* mutation strongly impaired *IRT1* mRNA accumulation compared with WT plants (Fig. 1*G*). Western blot analyses and quantification of chemiluminescence showed that IRT1 protein levels were also low in *fit* mutant and exactly mirrored the *IRT1* mRNA accumulation profile (Fig. 1 *H* and *I*), arguing against the existence of a FIT-dependent posttranslational regulation controlling IRT1 protein accumulation. Taken together, our results rule out by several complementary approaches the hypothesis of an iron-dependent degradation of IRT1.

***IRT1* Overexpression Leads to Metal Overaccumulation and Oxidative Stress.** Next, we evaluated the consequences of *IRT1* overexpression on plant metal content. We focused on transgenic lines harboring different levels of *IRT1* overexpression in roots and shoots, likely attributable to positional effects of the transgene, leading to modest *IRT1* overexpression in roots only (line 14), strong overexpression in roots and mild overexpression in shoots (line 9), and strong overexpression in both roots and shoots (lines 12 and 13) (Fig. 1 *B–E*). When grown in iron-replete conditions, WT and *irt1-1* plants harbored similar levels of iron in their leaves, whereas *irt1-1*/35S::IRT1 plants with high IRT1 levels, especially in leaves, displayed up to two- to threefold more iron (Fig. 2*A*). Levels of manganese, cobalt, and zinc in leaves were up to 10-fold higher in the various transgenic lines compared with both WT and *irt1-1* plants under the two iron regimes (Fig. 2*A*).

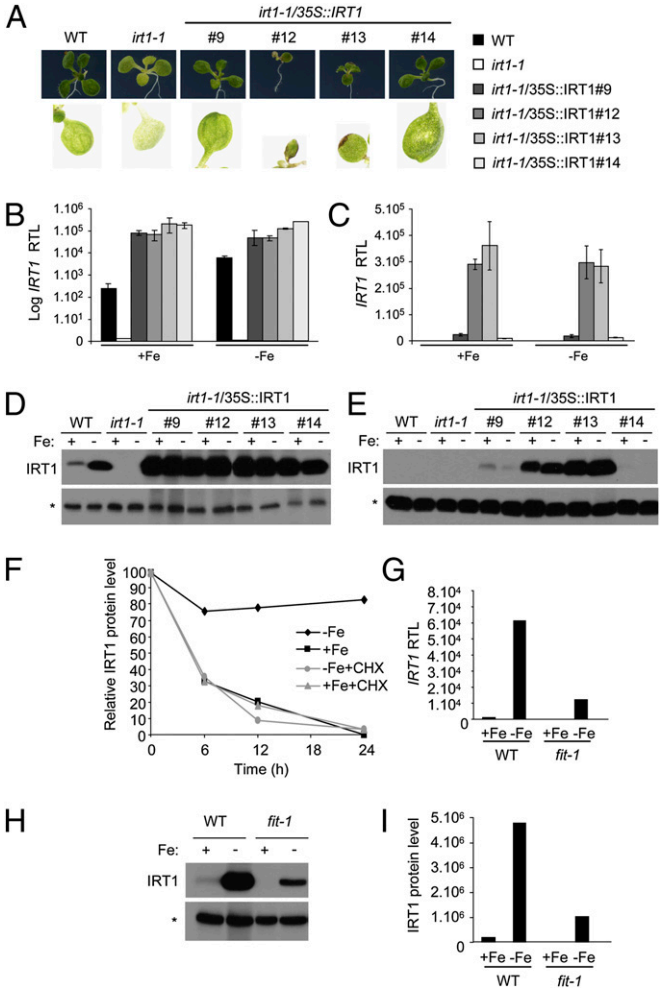

Fig. 1. Overexpression of *IRT1* leads to constitutive accumulation of IRT1 protein, regardless of iron supply. (*A*) Phenotype of plants constitutively expressing *IRT1*. Real-time quantitative RT-PCR monitoring of *IRT1* transcript accumulation in roots (*B*) and leaves (*C*) of WT, *irt1-1*, and *IRT1*-overexpressing plants. Experiments were performed on RNA extracted from 10-d-old plants transferred for 3 d on iron-sufficient (+Fe) or iron-deficient (−Fe) conditions. Four independent *irt1-1*/35S::IRT1 transgenic lines are shown. The results for *IRT1* expression in roots are shown as a logarithm of relative transcript levels to visualize *IRT1* induction by iron starvation in WT roots. RTL, relative transcript level. Error bars indicate SD. Western blot analyses monitoring of IRT1 protein levels in roots (*D*) and leaves (*E*) of WT, *irt1-1*, and *IRT1* overexpressors. The nonspecific band indicated with an asterisk serves as a loading control. (*F*) Half-life of endogenous IRT1 protein. Western blot analyses were performed using an anti-IRT1 antibody on total root protein extracts from WT −Fe plants transferred to +Fe or −Fe conditions in the presence or absence of CHX. (*G*) Quantitative RT-PCR monitoring of *IRT1* expression in WT and *fit-1* roots. Experiments were performed using RNA extracted from roots of 10-d-old plants transferred for 3 d in +Fe or −Fe conditions. The result from a representative experiment is shown. (*H*) IRT1 protein accumulation profile in roots from WT and *fit-1* plants grown in the same conditions as in *G*. The nonspecific band indicated with an asterisk serves as a loading control. (*I*) Quantification of the chemiluminescence signals from experiments presented in *H*.

Metal accumulation in *irt1-1*/35S::IRT1 transgenic roots reached dramatic levels, however. Compared with WT plants, strong *IRT1* overexpressors (lines 12 and 13) accumulated up to 300-fold more zinc, 110-fold more manganese, and 150-fold more cobalt (Fig. 2*B*). This indicates that *IRT1* overexpression leads to strong accumulation of metals in plants and shows that IRT1 protein activity is not affected by iron.

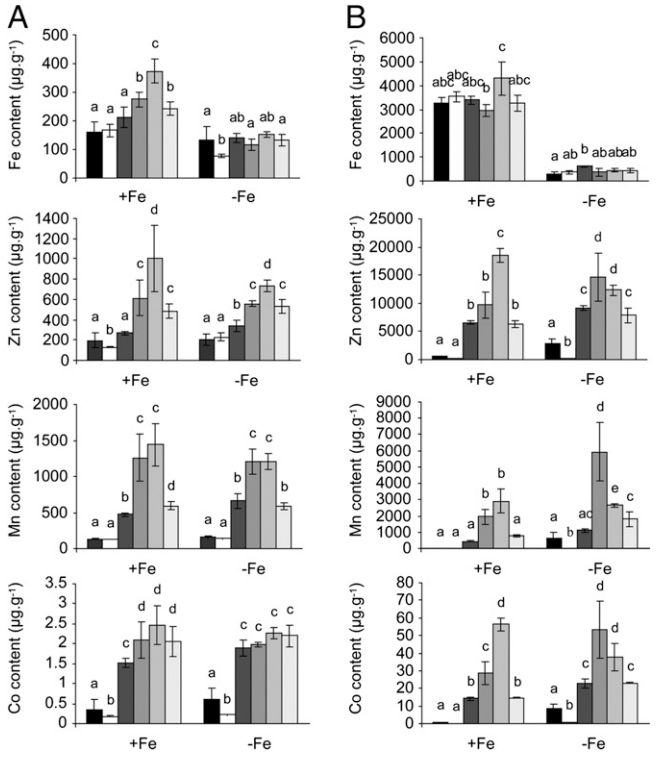

Fig. 2. *IRT1* overexpression leads to metal accumulation independent of iron nutrition. Metal content was determined by inductively coupled plasma mass spectrometry (ICP-MS) on leaves (*A*) and roots (*B*) from WT (black), *irt1-1* (white), *irt1-1*/35S::IRT1#9 (dark gray), *irt1-1*/35S::IRT1#12 (medium dark gray), *irt1-1*/35S::IRT1#13 (medium light gray), and *irt1-1*/35S::IRT1#14 (light gray) transgenic lines transferred to iron-sufficient (+Fe) or iron-deficient (−Fe) conditions for 5 d. Results are presented as mean ± SD ($n = 3$). Statistical differences were calculated by one-way ANOVA. Different letters indicate means that were statistically different by Tukey's multiple testing method ($P < 0.05$) for genotypes within a given growth condition (+Fe or −Fe).

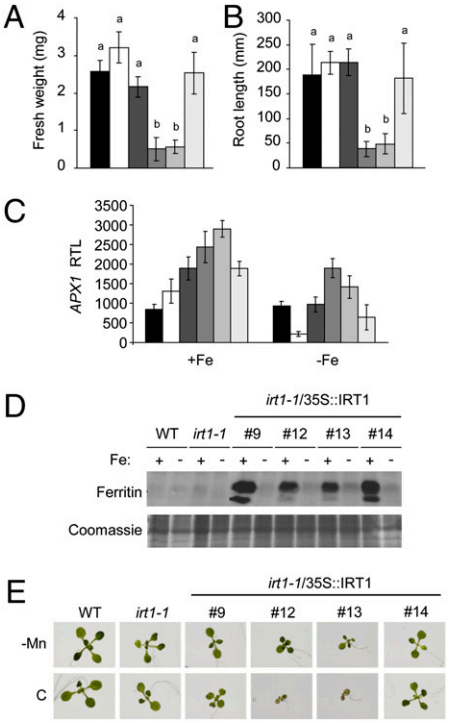

Fig. 3. IRT1-dependent metal accumulation affects growth and triggers oxidative stress responses. (*A*) Biomass measurements. Fresh weight was measured on 10-d-old WT (black), *irt1-1* (white), *irt1-1*/35S::IRT1#9 (dark gray), *irt1-1*/35S::IRT1#12 (medium dark gray), *irt1-1*/35S::IRT1#13 (medium light gray), and *irt1-1*/35S::IRT1#14 (light gray) transgenic plants grown in standard conditions. Results are presented as mean ± SD ($n = 10$). Statistical differences were calculated by one-way ANOVA. Different letters indicate means that were statistically different by Tukey's multiple testing method ($P < 0.05$). (*B*) Root length measurements in WT, *irt1-1*, and plants overexpressing *IRT1*. Results are presented as mean ± SD ($n = 15$). Statistical differences were calculated by one-way ANOVA. Different letters indicate means that were statistically different by Tukey's multiple testing method ($P < 0.05$). (*C*) Quantitative RT-PCR analyses monitoring *APX1* expression in leaves of WT, *irt1-1*, and *irt1-1*/35S::IRT1 transgenic lines. Experiments were performed using 10-d-old plants transferred for 3 d in iron-sufficient (+Fe) or iron-deficient (−Fe) conditions. Error bars represent SD. (*D*) Ferritin accumulation profile in leaves from WT, *irt1-1*, and *IRT1* overexpressors determined by Western blot analysis. Plants were grown as in *C*. (*E*) Phenotype of *IRT1* overexpressors in manganese-deficient conditions. WT, *irt1-1*, and *irt1-1*/35S::IRT1 transgenic plants were grown in standard conditions (C) or in manganese-poor (−Mn) medium for 12 d. Representative plants from each genotype are shown.

The strong overaccumulation of metals in *irt1-1*/35S::IRT1 plants had detrimental effects on growth. The *irt1-1*/35S::IRT1 transgenic lines that accumulated metals to dramatic levels (lines 12 and 13) clearly showed reduced biomass and root elongation (Fig. 3 *A* and *B*). Lines 9 and 14, which moderately accumulated metals, were not significantly affected, however. The iron overaccumulation in leaves displayed by the various *IRT1* overexpressors was accompanied by increased oxidative stress as measured by the accumulation of oxidative stress markers, such as the *APX1* ascorbate peroxidase mRNA (16) and the iron-binding protein ferritin (17), in leaves (Fig. 3 *C* and *D*). To evaluate if the metal accumulation directly caused *irt1-1*/35S::IRT1 growth defects, such plants were grown in manganese-limited conditions. Interestingly, only the transgenic lines that showed the strongest metal accumulation and growth reduction (lines 12 and 13) behaved better in the absence of manganese, indicating that dramatic metal overaccumulation is responsible for the growth reduction observed in such lines (Fig. 3*E*). Together, these results not only indicate that IRT1 is limiting for metal accumulation in roots but further highlight that tight control of IRT1 is required for optimal plant growth and development.

IRT1 Protein Localizes to the *Trans*-Golgi Network/Early Endosome. To investigate the subcellular localization and dynamics of endogenous IRT1 protein in roots, we used a direct immunocytochemical approach utilizing an anti-IRT1 antibody (18). Immunolocalization performed on root cross-sections from WT plants grown under iron sufficiency, conditions in which *IRT1* is not expressed (Fig. 1 *B* and *C*), or from iron-deficient *irt1-1* KO mutant showed no staining (Fig. 4*A*). WT plants grown under iron starvation, however, revealed a strong and specific IRT1 signal in epidermal cells (Fig. 4*A*) and, more specifically, in the trichoblastic cell lineage that develops into root hair cell files (Fig. S2). A closer examination at mature root hairs indicated that the IRT1-specific signal was concentrated in intracellular vesicles (Fig. 4*B*). Many IRT1-positive vesicles were located in close proximity to the plasma membrane because of the presence of a large central vacuole but with no staining found at the plasma membrane (Movie S1). The fixable FM4-64FX lipophilic dye that fluoresces on binding the plasma membrane was used to ensure that the plasma membrane was intact after the immunolocalization process, thus confirming that IRT1 does localize to intracellular vesicles (Fig. S3).

To identify the nature of IRT1-containing vesicles, we coimmunolocalized endogenous IRT1 protein with known markers of the endomembrane system. No colocalization or only very limited overlap was observed with the Golgi-localized Nucleotide Sugar

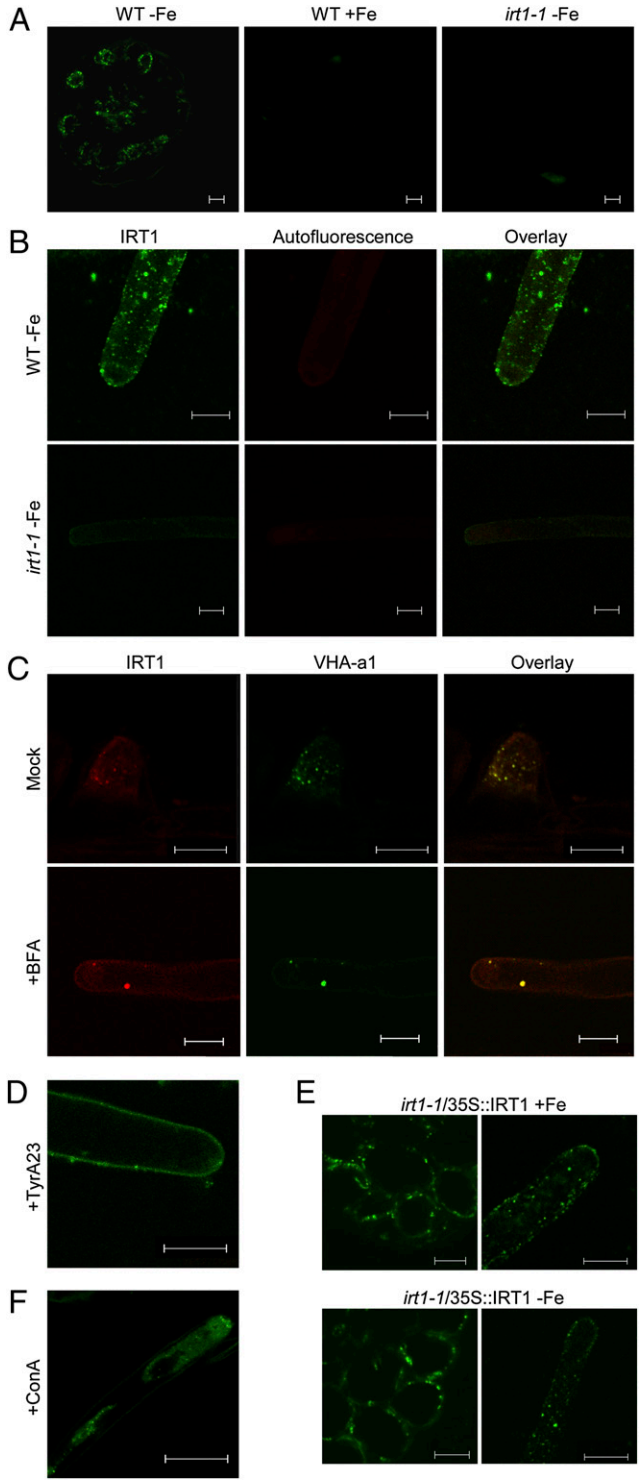

Fig. 4. IRT1 protein dynamically localizes to the early endosomes. (*A*) Immunofluorescence using anti-IRT1 antibody on root cross-section of WT and *irt1-1* plants. (*B*) Whole-mount immunolocalization monitoring IRT1 protein in root hairs of WT and *irt1-1* null mutant. The cell wall autofluorescence is shown in the red channel. (*C*) Colocalization of IRT1 with VHA-a1. Iron-starved VHA-a1–GFP transgenic plants were subjected to whole-mount immunolocalization using anti-GFP (Alexa488, green) and anti-IRT1 (Cy3, red) antibodies in the presence of mock (*Upper*) or BFA (*Lower*) treatment. Colocalization of IRT1 and VHA-a1 is shown in yellow in the overlay. (*D*) Immunolocalization of IRT1 in iron-starved WT plants following TyrA23 treatment. (*E*) Immunolocalization of IRT1 in root cross-sections (*Left*) and root hairs (*Right*) of *irt1-1*/35S::IRT1 plants grown in iron-sufficient (+Fe, *Upper*) or iron-deficient (–Fe, *Lower*) conditions. (*F*) Immunolocalization of IRT1 iron-starved WT plants after ConA treatment. (Scale bar = 10 μm.)

Transporter (19) or with the VAM3/SYP22 prevacuolar compartment/tonoplast-localized syntaxin (20, 21) (Fig. S4). Endogenous IRT1, however, colocalized with the *trans*-Golgi network/early endosome (TGN/EE) marker VHA-a1 (22) (Fig. 4*C*, *Upper*). Consistently, treatment with the fungal toxin Brefeldin A (BFA), which inhibits vesicular trafficking and recycling of endocytosed proteins to the plasma membrane in *Arabidopsis* roots (23), triggered the accumulation of IRT1 protein in large bodies (Fig. 4*C*, *Lower*), known as BFA bodies, which were positive for the presence of the BFA-sensitive VHA-a1 TGN/EE marker (22). Because IRT1 localizes to the crossroad of both the secretory and endocytic pathways, we investigated the effect of CHX on the BFA sensitivity of IRT1 trafficking. BFA bodies containing IRT1 were clearly observed in the absence of de novo protein synthesis, indicating that the pool of IRT1 found in BFA bodies came from preexisting intracellular pools of IRT1 (Fig. S5).

IRT1 Cycles Constitutively Between Early Endosomes and the Plasma Membrane and Is Targeted to the Vacuole for Degradation. Although the vast majority of the steady state of IRT1 protein is found in TGN/EE, we addressed the possibility that IRT1 may cycle between this compartment and the plasma membrane and be rapidly internalized by endocytosis. Iron-deficient roots were first exposed to Tyrphostin A23 (TyrA23), an inhibitor of cargo sorting into clathrin-coated vesicles (24, 25). Blocking clathrin-mediated endocytosis with TyrA23 allowed the visualization of IRT1-specific staining at the plasma membrane (Fig. 4*D*), suggesting that IRT1 undergoes endocytosis to keep the plasma membrane pool of IRT1 low, even under iron-limited conditions. The concomitant TyrA23-mediated depletion of intracellular IRT1 indicates that IRT1 is also recycled from early endosomes to the plasma membrane. The localization of IRT1 was unaffected by iron nutrition in root epidermal cells and root hairs of constitutively expressing IRT1 transgenic plants (Fig. 4*E*), indicating that IRT1 undergoes constant cycling between TGN/EE and the plasma membrane.

Plasma membrane proteins are degraded following endocytosis and subsequent trafficking to the lysosomes in mammals or to the vacuole in yeast/plants. To determine if IRT1 is degraded in the vacuole, iron-deficient roots were exposed to the v-ATPase inhibitor concanamycin A (ConA), a known inhibitor of plant vacuolar lytic activity (26, 27). ConA treatment triggered IRT1 protein accumulation in vacuoles of iron-deficient roots (Fig. 4*F*), further highlighting IRT1 dynamics in the cell and pointing to the vacuole as the site for IRT1 degradation. Analysis of constitutively expressing IRT1 transgenic plants unambiguously showed that IRT1 protein accumulates regardless of iron nutrition (Fig. 1*D*), suggesting that the trafficking of IRT1 to its degradation site occurs independent of its substrate.

Taken together, these observations indicate that IRT1 is found in the early endosomal compartments as a result of rapid endocytosis and slower recycling to the plasma membrane, where it likely performs iron uptake from the soil, and is addressed to the lytic vacuole for turnover. The abundance of IRT1 at the plasma membrane is therefore controlled by the specific contribution of each of these trafficking pathways.

IRT1 Is Monoubiquitinated in Vivo. To identify factors that control the trafficking or activity of IRT1, we performed a yeast two-hybrid screen looking for proteins interacting with the large cytosolic loop found between transmembrane domains III and IV in IRT1 (Fig. S6). Among the 119 IRT1-interacting clones identified, 15 contained a plasmid carrying the GAL4AD fused in-frame to the *Arabidopsis* Polyubiquitin10 gene (At4g05320). Polyubiquitin genes encode head-to-tail ubiquitin repeats that are posttranslationally processed to increase the pool of free ubiquitin in the cell (28). The interaction between the cytosolic loop of IRT1 and GAL4AD-ubiquitin, resulting from the processing

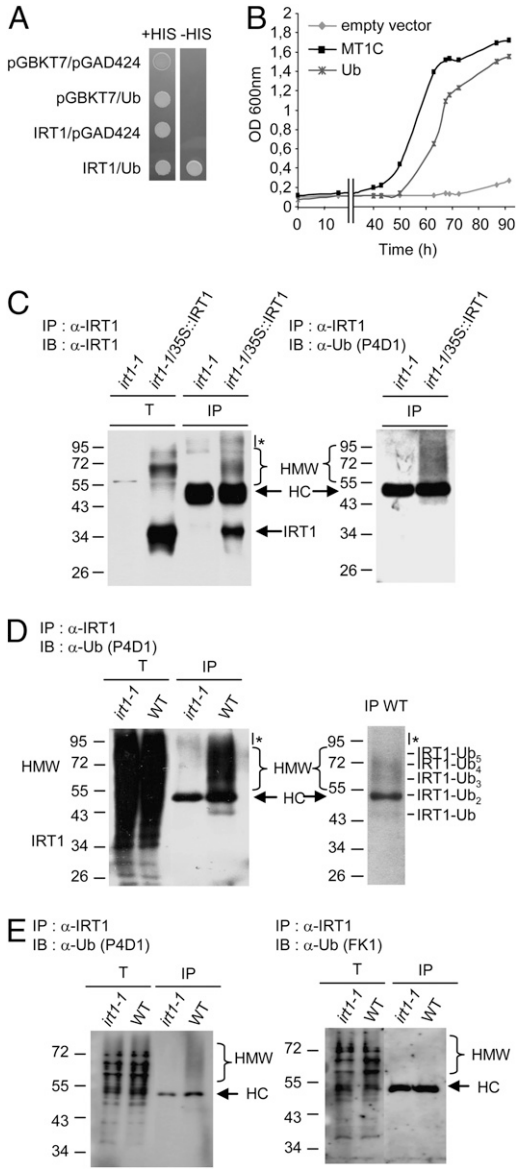

Fig. 5. Monoubiquitin-dependent trafficking and turnover of IRT1. (*A*) Yeast two-hybrid test monitoring interaction between the IRT1 loop and ubiquitin. The corresponding empty vectors were used as controls. The interaction is revealed by the activation of *HIS3* transcription and growth on −HIS medium. (*B*) Functional cadmium sensitivity test in yeast. Yeast cells expressing *IRT1* were transformed with empty vector, polyubiquitination, or the metallothionein MT1C-positive control and were grown in the presence of 0.2 μM cadmium. Yeast growth was followed by measuring the optical density over 96 h. (*C*) In vivo ubiquitination analyses of IRT1. Immunoprecipitation was performed using an anti-IRT1 antibody on solubilized root protein extracts (T) from iron-replete *irt1-1*/35S::IRT1 or *irt1-1* plants and subjected to immunoblotting with an anti-IRT1 antibody (*Left*) or the antiubiquitin (P4D1) antibody that recognizes monoubiquitination and polyubiquitination (*Right*). IB, immunoblotting; IP, immunoprecipitation. The heavy chain of IRT1 antibody and the high-molecular-weight smear specific for IRT1 immunoprecipitates are shown. HC, heavy chain; HMW, high molecular weight. The asterisk indicates aspecific signals observed in both *irt1-1* and *irt1-1*/35S::IRT1 lanes. (*D*) Ubiquitination analyses of endogenous IRT1. IRT1-immunoprecipitated fractions from WT and *irt1-1* iron-deficient plants were subjected to Western blot analysis with the antiubiquitin (P4D1) antibody. (*Right*) Lower exposure, with several bands corresponding to ubiquitinated forms of IRT1, each migrating ~9 kDa apart. (*E*) IRT1 monoubiquitination analyses. IRT1 immunoprecipitates were subjected to Western blot analysis with both the antimonoubiquitination/polyubiquitination-specific (P4D1, *Left*) and polyubiquitination-specific (FK1, *Right*) antibodies.

of the five ubiquitin repeats from Polyubiquitin10, was confirmed in a secondary yeast two-hybrid test (Fig. 5*A*). Such interaction reveals a possible covalent linkage of ubiquitin to amino acid residues found in the cytosolic loop of IRT1 by yeast E3 ligases. To investigate the role of ubiquitin and ubiquitination processes, we overexpressed ubiquitin in IRT1-expressing yeast cells. Yeast cells with altered free ubiquitin are known to harbor lower levels of proteins subjected to ubiquitin-dependent degradation. This includes plasma membrane proteins undergoing ubiquitin-dependent endocytosis and degradation, such as the Can1 arginine transporter (29). Consistent with the ability of IRT1 to transport cadmium (3, 30, 31), *IRT1* expression in yeast conferred hypersensitivity to external cadmium (Fig. S7). When transformed with Polyubiquitin10, to overproduce ubiquitin, or the cadmium-binding Metallothionein1C positive control (32), IRT1-expressing yeast grew in the presence of toxic amounts of cadmium, suggesting that increasing free ubiquitin pools impaired the IRT1-mediated cadmium hypersensitivity (Fig. 5*B*). Taken together, these results indicate that IRT1 directly interacts with ubiquitin in yeast, likely via ubiquitination of IRT1 protein, and that such posttranslational modification affects its ability to transport metals.

We next addressed whether endogenous IRT1 protein was ubiquitinated *in planta*. IRT1 was immunoprecipitated from *irt1-1*/35S::IRT1 plants or *irt1-1* as a negative control, using the anti-IRT1 antibody. Western blot analyses of IRT1 immunoprecipitates with the anti-IRT1 antibody revealed a 36-kDa band corresponding to IRT1, as well as a high-molecular-weight smear (Fig. 5*C*, *Left*) typical of ubiquitinated forms of multispanning transmembrane proteins (29, 33–35). IRT1 immunoprecipitates were specifically enriched in IRT1 protein as attested by the absence of the abundant membrane-localized root aquaporin PIP2 (Fig. S8). When probed with an antiubiquitin antibody (P4D1) that recognizes both monoubiquitin and polyubiquitin chains, IRT1-immunoprecipitates from *irt1-1*/35S::IRT1 plants showed the same high-molecular-weight smear, whereas no signal was detected for *irt1-1*, indicating that IRT1 is likely posttranslationally modified by ubiquitin residues in vivo (Fig. 5*C*, *Right*). Endogenous IRT1 protein immunoprecipitated from iron-deficient WT plants is also ubiquitinated in vivo (Fig. 5*D*, *Left*). When underexposed, several bands likely corresponding to ubiquitinated forms of IRT1, each migrating 9 kDa apart, were revealed specifically in IRT1 immunoprecipitates (Fig. 5*D*, *Right*). To strengthen our conclusions that IRT1 is ubiquitinated, we performed similar experiments using a more stringent solubilization protocol before immunoprecipitation. Such conditions still allowed the visualization of ubiquitination signals in IRT1 immunoprecipitates (Fig. S9). Together, these observations strongly suggest that IRT1 is posttranslationally modified by ubiquitination in vivo and carries a discrete number of ubiquitin moieties, although we cannot formally exclude that such ubiquitination signals may come from a possible IRT1-interacting protein coimmunoprecipitated in our conditions. Ubiquitination of endogenous IRT1 was not detected using an antibody (FK1) specific for polyubiquitination (Fig. 5*E*, *Right*), although global polyubiquitination intensity from inputs looked comparable to P4D1 (Fig. 5*E*, *Left*), indicating that IRT1 protein is monoubiquitinated in vivo on several lysine residues.

Monoubiquitin-Dependent Trafficking and Turnover of IRT1. To address the functional relevance of IRT1 monoubiquitination in vivo, we performed site-directed mutagenesis on the two lysine residues (K154 and K179) found in the IRT1 cytosolic loop that interacts with ubiquitin in the yeast two-hybrid. Expression of 35S::IRT1$_{K154R,K179R}$ in the *irt1-1* background led to an extreme growth reduction, the presence of necrotic spots on seedlings highlighting massive oxidative stress, and rapid lethality for most of the transgenic lines (>150 lines) (Fig. 6*A*). This clearly indicates that the K154R,K179R mutation dramatically exacerbates the negative effect of *IRT1* overexpression, and thereby IRT1

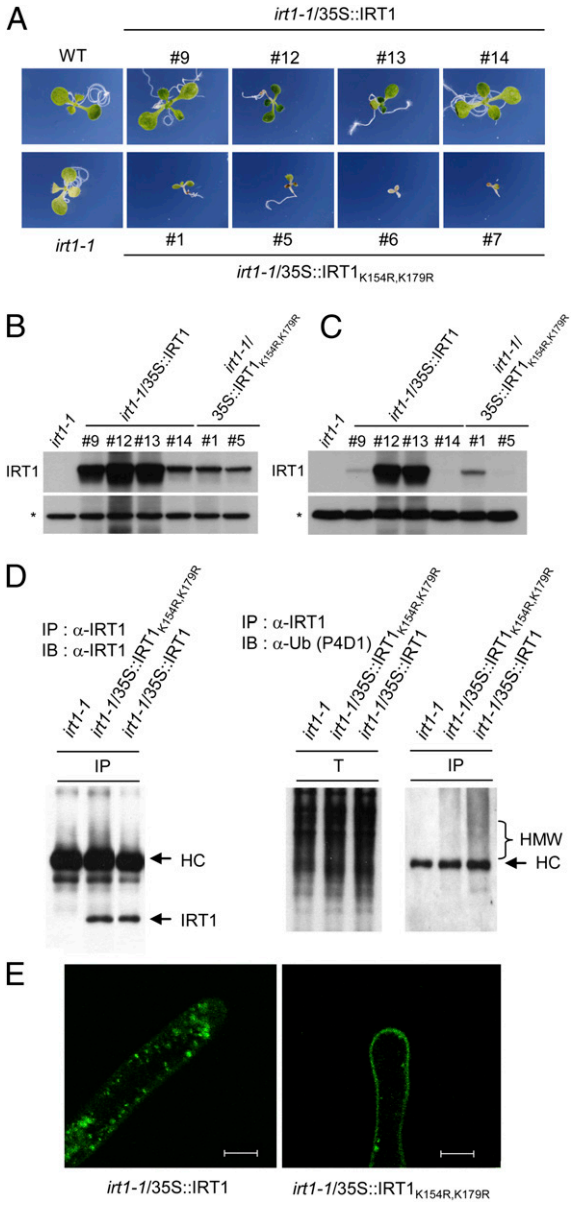

Fig. 6. Monoubiquitination of two lysine residues controls IRT1 localization and degradation. (*A*) Phenotypic analysis of seedlings from independent transgenic lines expressing *IRT1* and $IRT1_{K154R,K179R}$ under the control of 35S promoter. Western blot analyses monitoring IRT1 protein accumulation in roots (*B*) and shoots (*C*) of *irt1-1*/35S::IRT1 and *irt1-1*/35S::$IRT1_{K154R,K179R}$ transgenic lines. (*D*) In vivo ubiquitination profile of IRT1. IRT1 immunoprecipitates from *irt1-1*, *irt1-1*/35S::IRT1, and *irt1-1*/35S::$IRT1_{K154R,K179R}$ plants were subjected to Western blot analysis with the anti-IRT1 (*Left*) and the antiubiquitin (P4D1, *Right*) antibodies. IB, immunoblotting; IP, immunoprecipitation. (*E*) Whole-mount immunolocalization analyses of IRT1 in *irt1-1*/35S::IRT1 and *irt1-1*/35S::$IRT1_{K154R,K179R}$ plants. (Scale bar = 10 μm.)

activity. The *irt1-1*/35S::$IRT1_{K154R,K179R}$ lines expressing low levels of mutated IRT1 survived and produced few seeds when grown in soil, indicating complementation of the *irt1-1* phenotype (Fig. S10). The *irt1-1*/35S::$IRT1_{K154R,K179R}$ lines were clearly more affected than their *irt1-1*/35S::IRT1 counterparts (Fig. 6*A*), however, although expressing IRT1 at lower levels in both roots (Fig. 6*B*) and shoots (Fig. 6*C*). The *irt1-1*/35S::$IRT1_{K154R,K179R}$ plants harbored decreased IRT1 ubiquitination intensity and levels (Fig. 6*D*), indicating that residues K154 and K179 are likely direct ubiquitination targets in vivo. Because monoubiquitination of plasma membrane proteins has been shown in yeast and mammals to be a prerequisite for endocytosis and degradation (36), we investigated the subcellular localization of IRT1 in *irt1-1*/35S::$IRT1_{K154R,K179R}$ transgenics. In contrast to what is observed in WT (Fig. 4*B*) or *irt1-1*/35S::IRT1 (Fig. 4*E*) plants, IRT1 is readily found at the plasma membrane in *irt1-1*/35S::$IRT1_{K154R,K179R}$ plants (Fig. 6*E*). The increased plasma membrane localization of $IRT1_{K154R,K179R}$ explains why *irt1-1*/35S::$IRT1_{K154R,K179R}$ plants are more severely affected than *irt1-1*/35S::IRT1 lines, likely by metal overload. Together, these results clearly establish a role for monoubiquitination in IRT1 dynamics and turnover, and highlight the necessity for tight control of IRT1 levels at the plasma membrane for proper iron and metal homeostasis.

Discussion

In this report, we show that IRT1 is primarily regulated at the transcriptional level by iron starvation, excluding the existence of iron-dependent posttranscriptional regulatory events targeting IRT1 protein accumulation. Our work also unravels that IRT1 is localized to TGN/EE compartments as a consequence of the constant and rapid endocytosis of the plasma membrane pool of IRT1 mediated by monoubiquitination of cytosol-exposed lysine residues. More importantly, we demonstrate that the subcellular localization and abundance of IRT1 are crucial for proper iron and metal uptake as well as plant growth and development.

IRT1 was shown to be posttranscriptionally regulated by iron, with iron-replete conditions triggering the disappearance of IRT1 protein (8). Whether this regulation was the consequence of translational or posttranslational control was not known. However, some researchers suggested that IRT1 would undergo iron-dependent destabilization based on the analogy with the yeast ZRT1 zinc transporter (8). We demonstrated by several complementary approaches that *IRT1* is not posttranscriptionally regulated by iron. Previous conclusions were drawn using constitutive expression of a truncated version of IRT1 (8), lacking 9 amino-acids in the N-terminus, where a putative signal peptide resides, in wild-type Arabidopsis plants expressing endogenous *IRT1*. Such a truncated form of IRT1 is certainly misfolded and unstable as a result of the endoplasmic reticulum-associated degradation quality control (37). The absence of IRT1 protein accumulation in iron-sufficient WT/35S::$IRT1_{trunc}$ plants (8), originally interpreted as evidence of *IRT1* posttranscriptional regulation by iron, therefore reflects the expression pattern of endogenous IRT1 protein, because transgene expression was assessed in a WT background. Instead, IRT1 undergoes constant monoubiquitination-dependent endocytosis and targeting to the vacuole for proper turnover.

The localization of IRT1 to TGN/EE compartments appears unexpected at first, because IRT1 was shown to mediate iron uptake in plants or when overexpressed in yeast (3, 38). The dynamic nature of IRT1 protein in the cell is only revealed when plants are challenged with drugs interfering with internalization and recycling of plasma membrane proteins, or when two ubiquitinated lysine residues in IRT1 are mutated (Fig. 7). This suggests that even under iron starvation, the pool of IRT1 at the plasma membrane is low and tightly controlled by ubiquitin-dependent trafficking. The fact that *IRT1* overexpression did not increase IRT1 plasma membrane pools to a detectable level also argues for a major role of endocytosis to keep IRT1 low at the cell surface. The dramatic metal accumulation displayed by plants overexpressing *IRT1* therefore likely comes from expanded expression territories for IRT1 in roots compared with WT plants. The rationale for having large quantities of the transporter in TGN/EE is not clear, because none of the growth conditions tested so far led to a reallocation of the IRT1 pool to the plasma membrane. Iron starvation may modify the pace of IRT1 internalization and recycling, with the steady state of IRT1 protein

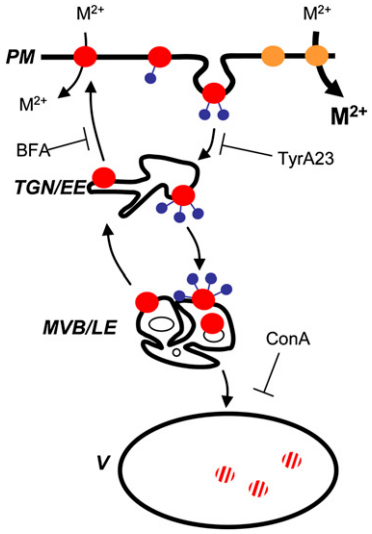

Fig. 7. Diagram illustrating the dynamics of IRT1 protein in the cell. The continuous monoubiquitination-dependent cycling of IRT1 (red circles) between the plasma membrane (PM) and early endosomes (TGN/EE) controls its subcellular distribution and transport of divalent metals (M^{2+}). A fraction of monoubiquitinated endocytosed IRT1 protein is not recycled to the plasma membrane and is constantly sent for degradation in the vacuole (V) via multivesicular bodies (MVBs/LEs), thereby controlling IRT1 protein total levels. Inhibition of endocytosis (TyrA23), recycling to the plasma membrane (BFA), degradation in the vacuole (ConA), and mutation of residues K154 and K179 (orange circles) interfere with intracellular distribution of IRT1.

still in TGN/EE, to increase iron and metal uptake at the plasma membrane. However, iron nutrition had no effect on other metal accumulation in IRT1 overexpressor lines, suggesting that iron nutrition affects neither the dynamic localization of IRT1 nor its activity.

Only a very few membrane proteins, such as the auxin efflux carrier PIN2, the water channel aquaporin PIP2;1, and the flagellin receptor FLS2, were experimentally shown to be ubiquitinated in plants and proposed by researchers to undergo proteasome-dependent degradation (13–15). Our work not only shows that IRT1 is ubiquitinated in vivo but demonstrates that monoubiquitination of IRT1 triggers its trafficking to the vacuole, where it is degraded as part of the constitutive IRT1 turnover. Although ubiquitination of serine, threonine, and cysteine has recently been reported (39, 40), we favor the model in which the cytosol-exposed lysine residues K154 and K179, which are important for IRT1 ubiquitination, are direct ubiquitin attachment sites in IRT1, and therefore control IRT1 dynamics. The extreme lethality observed in *irt1-1*/35S::$IRT1_{K154R,K179R}$ transgenic plants also indicates that the control of IRT1 protein levels and localization by ubiquitination is critical for proper iron homeostasis of plant root cells and the whole organism. Monoubiquitination-dependent trafficking of IRT1 is therefore reminiscent of what is observed for receptor and transporter endocytosis in yeast and mammals, where ubiquitination triggers internalization and sorting of membrane proteins in multivesicular bodies/late endosomes (MVBs/LEs) for targeting and degradation in the vacuole/lysosomes (10–12). Proteasome activity has been shown to interfere with plasma membrane protein degradation in animal and yeast cells via altered targeting of membrane proteins to the vacuole/lysosomes (41–44). This likely explains why ubiquitinated PIP2;1, PIN2, and FLS2 are stabilized following MG132 treatment, and therefore why they were suggested to undergo proteasome-mediated degradation (13–15). Our work now establishes monoubiquitination-dependent endocytosis and trafficking as a conserved mechanism to target plasma membrane proteins to the vacuole for degradation in plants.

Studies in yeast and mammals have demonstrated that ubiquitination occurs at various steps in endocytosis to control plasma membrane protein internalization and sorting into internal vesicles of MVBs/LEs on their way to the vacuole/lysosome (36). In addition to residues K154 and K179, in which substitution to arginine is sufficient to abolish monoubiquitination-dependent trafficking, IRT1 likely carries monoubiquitination moieties on other cytosol-exposed lysine residues. How differential ubiquitination influences the dynamic of IRT1 along the endocytic pathway remains an open question. Although single monoubiquitination appears sufficient for internalization of plasma membrane proteins (10–12), multiple monoubiquitinations of IRT1 may increase the rate of such a process, as observed for the Fur4 yeast uracil permease (33, 45). The presence of pools of IRT1 decorated with different numbers of monoubiquitination residues may also reflect a hierarchy in ubiquitinated residues. Different monoubiquitinated regions of IRT1 may be selectively recognized by ubiquitin-binding proteins, thereby controlling IRT1 destination along the endocytic pathway and fate (Fig. 7). This scenario is supported in mammals by the observation that the E3-ubiquitin ligase Cbl promotes progressive ubiquitination of activated EGFR throughout the endocytic route (10). The relative contribution of each monoubiquitination residue in the pace of IRT1 internalization or in the sorting of IRT1 on its way to the vacuole will have to be studied by careful examination of IRT1 levels, localization, and dynamics in transgenic plants expressing single mutated versions of IRT1 in cytosol-facing lysine residues.

Conclusion

The data presented here show that ubiquitin-dependent endocytosis and degradation are conserved in plants and, more specifically, highlight the importance of posttranslational control of IRT1 to keep iron and heavy metal uptake in check. The role of monoubiquitination in other biological functions, such as auxin transport, brassinosteroid signaling, and pathogen response, where plasma membrane transporters and receptors are known to undergo endocytosis (13, 46, 47), will have to be addressed in the future.

Methods

Plant Material and Growth Conditions. The *irt1-1* (3) (Wassilevskija ecotype), *fit-1* (5) (Wassilevskija ecotype), corresponding WT, and different transgenic lines used in this study were grown in sterile conditions on vertical plates at 21 °C with 16-h light/8-h dark cycles. Plants were grown exactly as previously described (18). For expression analyses, plants were cultivated in the conditions described above for 7 d and then transferred on iron-sufficient (50 μM Fe-EDTA) or iron-deficient (300 μM Ferrozine [3-(2-pyridyl)-5,6-diphenyl-1,2,4-triazine sulfonate], a strong iron chelator) medium for an additional 3 d. For in-plate CHX treatments, plants were transferred on either iron-sufficient or iron-deficient medium in the presence or absence of 100 μM CHX. For immunolocalization studies, iron starvation was applied by directly germinating seeds on half-strength Murashige and Skoog (MS) medium lacking exogenous iron to preserve root integrity. For confocal microscopy analyses, inhibitors (33 μM TyrA23, 50 μM BFA, and 0.5 μM ConA) or mock inhibitors were applied in liquid 1/2 MS medium before imaging. All reagents were purchased from Sigma Aldrich.

Expression of *IRT1* in Transgenic Plants. Full-length *IRT1*, containing the 5′- and 3′-untranslated regions as well as the two introns, was amplified by PCR using genomic DNA as a template and the IRT1 FL F and IRT1 FL R primers (Table S1). *IRT1* was cloned in the pBIBHygro binary vector under the control of 35S promoter. To generate *IRT1* mutant versions, site-directed mutagenesis was carried out by PCR using the $IRT1_{K154R}$ F, $IRT1_{K154R}$ R, $IRT1_{K179R}$ F, and $IRT1_{K179R}$ R primers, according to the instructions for Stratagene's QuikChange Site-Directed Mutagenesis kit (Agilent Technologies). The different constructs were transferred to *Agrobacterium tumefaciens* strain GV3101 and transformed into *irt1-1* mutant plants by floral dipping.

RNA Extraction and Real-Time Quantitative PCR. Total RNA was extracted using TRIzol reagent (Invitrogen) and purified using the RNeasy MinElute Cleanup Kit (Qiagen) after DNase treatment (Qiagen). The integrity of DNA-free RNA was verified by agarose gel electrophoresis, and an equal amount of total RNA (2 μg) was used for RT with anchored oligo(dT23). Real-time PCR was performed exactly as previously described (18), using gene-specific and control primers (Table S1). The experiments were done in three biological replicates, with each containing two technical replicates.

Protein Extraction and Western Blot Analysis. Western blot analyses were performed on total proteins exactly as previously described (18). Immunodetection of IRT1 protein was performed using an affinity-purified anti-peptide IRT1 antibody diluted 1:5,000. The IRT1 polyclonal antibody was raised in rabbits against two synthetic peptides, H2N-CMASNSALLMKTIFLV-CONH2 and H2N-CPANDVTLPIKEDDSS-CONH2 (18). Immunodetection of ferritins was performed using an antiferritin antibody recognizing all four isoforms (48). The PIP2 aquaporin was monitored using a primary antibody raised against a 17-amino acid C-terminal peptide of AtPIP2;1 (49). Ubiquitin modifications were detected using the P4D1 mouse monoclonal antibody (IgG) diluted 1:1,000 (Santa Cruz Biotechnology), which recognizes both monoubiquitination and nonspecific lysine linkage polyubiquitination chains, and the FK1 mouse monoclonal antibody (IgM) diluted 1:1,000 (Millipore), which specifically recognizes polyubiquitination chains. Next, the membranes were washed in blocking buffer three times and incubated with anti-rabbit IgG conjugated to alkaline phosphatase (Promega) to detect anti-IRT1, antiferritin, and anti-PIP2 primary antibodies, or with anti-mouse IgG and anti-mouse IgM conjugated to alkaline phosphatase (Sigma Aldrich) to detect P4D1 and FK1 antibodies, respectively. All the secondary antibodies were diluted 1:20,000 in blocking buffer. After several washes, membranes were incubated in Immobilon Western Chemiluminescent AP substrate (Millipore) and chemiluminescence was revealed on BioMax XAR film (Kodak) or using the LAS3000 Imaging System (Fujifilm) for accurate quantification.

Immunolocalization. Immunolocalization on root cross-sections was performed using 7-d-old plants fixed for 1 h in 4% (wt/vol) paraformaldehyde (PFA), mounted in 3% (wt/vol) agarose, and cut with a Vibratome (Microm) in ~70-μm sections. Sections were blocked overnight at 4 °C in PBS-Triton 0.05% (PBS-T) and 2% (wt/vol) BSA before overnight incubation with the anti-IRT1 antibody at 4 °C in PBS-T. Sections were washed three times for 10 min in PBS-T before incubation with the secondary (Alexa488–anti-rabbit goat antibody, MolecularProbes A11008; Invitrogen) and then tertiary (Alexa488–anti-goat donkey antibody, MolecularProbes A11055; Invitrogen) antibodies for 1 h each at room temperature in PBS-T. After washes, sections were mounted in antifade medium before imaging.

Whole-mount immunolocalizations were performed using 7-d-old plants fixed for 1 h in 4% (wt/vol) PFA, gently placed on superfrost slides (5069M; ThermoScientific), and then dried overnight at 37 °C. The immunolocalization on slides was performed exactly as described (50), using anti-IRT1 and anti-GFP (11814460001; Roche) primary antibodies and the corresponding secondary antibodies (Alexa488–anti-rabbit antibody, MolecularProbes A11070, Invitrogen; Alexa488–anti-mouse antibody, MolecularProbes A11017 Invitrogen; and Cy3–anti-rabbit antibody, 11-167-003, ImmunoResearch). After mounting in antifade medium, intact root hairs or root cross-sections were imaged.

Confocal microscopy analyses were carried out using Leica SP2 and Zeiss LSM510 Meta confocal microscopes. Excitation/detection parameters for Alexa488 and cy3 were 488/501–530 nm and 543/568–737 nm, respectively.

Elemental Analyses. Tissues were desorbed by washing for 10 min with 2 mM $CaSO_4$ and 10 mM EDTA and then rinsed for 5 min with deionized water. Samples were dried at 80 °C for 2 d. For mineralization, tissues were digested completely (1–3 h) in 70% (vol/vol) HNO_3 at 120 °C. Elemental analyses were performed by ICP-MS.

Yeast Two-Hybrid Screen. A fragment of the *IRT1* cDNA, encoding the cytosolic loop of IRT1 (amino acids 146–194), was cloned into the pGBKT7 vector (Clontech) and transformed in the AH109 yeast strain. The resulting yeast cells were then transformed with plasmid DNAs derived from the CD4-10 *Arabidopsis* cDNA library prepared with roots and shoots of 4-wk-old plants. Approximately 10^6 transformants were screened for activation of the HIS3 and LacZ reporters. Positive clones were sequenced, and interesting candidates in which GAL4AD was in frame with the corresponding cDNA were rescued. Candidate clones isolated from the screen were then individually retransformed in yeast cells expressing GALDB alone or the GAL4DB-IRT1 prey fusion for confirmation.

Yeast Cadmium Sensitivity Assay. Two copies of the *IRT1* coding sequence were cloned in YIpDCE1 under the control of the strong PGK promoter. The cassette was stably integrated at the *ADE2* locus in W303 WT yeast. IRT1-expressing yeast was subsequently transformed with the pFL61 empty vector, pFL61-polyubiquitination and pFL61-MT1C, expressing the metallothionein 1C that confers resistance to cadmium (32). Growth in the presence of cadmium was assessed in liquid culture containing 0.2 μM cadmium over 4 d.

Immunoprecipitation. Roots of plants cultivated in the conditions described above were ground in liquid nitrogen and resuspended in RIPA buffer [50 mM Tris-HCl (pH 7.5), 150 mM NaCl, 0.5% sodium deoxycholate, 1% Nonidet P-40, 0.1% SDS, 10 mM *N*-ethylmaleimide, and protease inhibitor (Roche) mixture according to the manufacturer's instructions]. After centrifugation at 3,800 × *g* for 10 min at 4 °C, the resultant supernatant was collected and solubilization was continued for 2 h at 4 °C on a rotating wheel. Samples were centrifuged at 100,000 × *g* for 45 min at 4 °C to remove membrane fraction, and the supernatant was incubated with the anti-IRT1 antibody for 16 h at 4 °C on a rotating wheel. After incubation with 50 μL of magnetic Dynabeads Protein A (Invitrogen) for 2 h at 4 °C, the IgG–Dynabeads Protein A complexes were captured according to the manufacturer's instructions by using a magnet. Beads were washed four times with 0.5 mL of RIPA, followed by four washes with 0.5 mL of PBS. The IRT1–IgG complexes were eluted from the beads by adding 2× SDS sample buffer and heating at 65 °C for 10 min. Collected fractions were analyzed by Western blots as described above. For stringent solubilization conditions, microsomes were resuspended in a modified RIPA buffer containing 1% SDS. Once solubilized, proteins were heated at 65 °C for 10 min before dilution to 0.1% SDS and immunoprecipitation.

Statistical Analysis. One-way ANOVA was used for parametric or nonparametric comparison of means for statistical analyses of metal content, biomass determination, and root length measurements. Significant differences were further analyzed using Tukey's parametric or nonparametric test to identify differences between genotypes. All these tests used an α-value of 0.05 and were done with the R software (R Development Core Team).

ACKNOWLEDGMENTS. Véronique Vacchina and Ryszard Lobinsky are thanked for their assistance with ICP-MS analyses. We thank Ullas Pedmale, Christophe Maurel, and Frédéric Gaymard for providing antibodies and Yvon Jaillais for critical reading of the manuscript. This work was supported by a PhD fellowship from the French Ministry of National Education, Research, and Technology (to M.B.), the Odysseus program of the Research Foundation of Flanders (to S.R and J.F.), and Grant CDA0005/2007 from the Human Frontier Science Program Organization and Grant ANR-08-JCJC-0058 from the Agence Nationale de la Recherche (to G.V.).

1. Curie C, Briat JF (2003) Iron transport and signaling in plants. *Annu Rev Plant Biol* 54: 183–206.
2. Briat JF, et al. (1995) Cellular and molecular aspects of iron metabolism in plants. *Biol Cell* 84:69–81.
3. Vert G, et al. (2002) IRT1, an Arabidopsis transporter essential for iron uptake from the soil and for plant growth. *Plant Cell* 14:1223–1233.
4. Henriques R, et al. (2002) Knock-out of Arabidopsis metal transporter gene IRT1 results in iron deficiency accompanied by cell differentiation defects. *Plant Mol Biol* 50:587–597.
5. Colangelo EP, Guerinot ML (2004) The essential basic helix-loop-helix protein FIT1 is required for the iron deficiency response. *Plant Cell* 16:3400–3412.
6. Jakoby M, Wang HY, Reidt W, Weisshaar B, Bauer P (2004) FRU (BHLH029) is required for induction of iron mobilization genes in Arabidopsis thaliana. *FEBS Lett* 577: 528–534.
7. Yuan YX, Zhang J, Wang DW, Ling HQ (2005) AtbHLH29 of Arabidopsis thaliana is a functional ortholog of tomato FER involved in controlling iron acquisition in strategy I plants. *Cell Res* 15:613–621.
8. Connolly EL, Fett JP, Guerinot ML (2002) Expression of the IRT1 metal transporter is controlled by metals at the levels of transcript and protein accumulation. *Plant Cell* 14:1347–1357.
9. Bonifacino JS, Weissman AM (1998) Ubiquitin and the control of protein fate in the secretory and endocytic pathways. *Annu Rev Cell Dev Biol* 14:19–57.
10. Haglund K, et al. (2003) Multiple monoubiquitination of RTKs is sufficient for their endocytosis and degradation. *Nat Cell Biol* 5:461–466.
11. Shih SC, Sloper-Mould KE, Hicke L (2000) Monoubiquitin carries a novel internalization signal that is appended to activated receptors. *EMBO J* 19:187–198.
12. Dupré S, Urban-Grimal D, Haguenauer-Tsapis R (2004) Ubiquitin and endocytic internalization in yeast and animal cells. *Biochim Biophys Acta* 1695:89–111.

13. Abas L, et al. (2006) Intracellular trafficking and proteolysis of the Arabidopsis auxin-efflux facilitator PIN2 are involved in root gravitropism. *Nat Cell Biol* 8:249–256.
14. Göhre V, et al. (2008) Plant pattern-recognition receptor FLS2 is directed for degradation by the bacterial ubiquitin ligase AvrPtoB. *Curr Biol* 18:1824–1832.
15. Lee HK, et al. (2009) Drought stress-induced Rma1H1, a RING membrane-anchor E3 ubiquitin ligase homolog, regulates aquaporin levels via ubiquitination in transgenic Arabidopsis plants. *Plant Cell* 21:622–641.
16. Fourcroy P, Vansuyt G, Kushnir S, Inzé D, Briat JF (2004) Iron-regulated expression of a cytosolic ascorbate peroxidase encoded by the APX1 gene in Arabidopsis seedlings. *Plant Physiol* 134:605–613.
17. Ravet K, et al. (2009) Ferritins control interaction between iron homeostasis and oxidative stress in Arabidopsis. *Plant J* 57:400–412.
18. Séguéla M, Briat JF, Vert G, Curie C (2008) Cytokinins negatively regulate the root iron uptake machinery in Arabidopsis through a growth-dependent pathway. *Plant J* 55: 289–300.
19. Rollwitz I, Santaella M, Hille D, Flügge UI, Fischer K (2006) Characterization of AtNST-KT1, a novel UDP-galactose transporter from Arabidopsis thaliana. *FEBS Lett* 580: 4246–4251.
20. Sanderfoot AA, Raikhel NV (1999) The specificity of vesicle trafficking: Coat proteins and SNAREs. *Plant Cell* 11:629–642.
21. Robert S, et al. (2008) Endosidin1 defines a compartment involved in endocytosis of the brassinosteroid receptor BRI1 and the auxin transporters PIN2 and AUX1. *Proc Natl Acad Sci USA* 105:8464–8469.
22. Dettmer J, Hong-Hermesdorf A, Stierhof YD, Schumacher K (2006) Vacuolar H+-ATPase activity is required for endocytic and secretory trafficking in Arabidopsis. *Plant Cell* 18: 715–730.
23. Geldner N, et al. (2003) The Arabidopsis GNOM ARF-GEF mediates endosomal recycling, auxin transport, and auxin-dependent plant growth. *Cell* 112:219–230.
24. Banbury DN, Oakley JD, Sessions RB, Banting G (2003) Tyrphostin A23 inhibits internalization of the transferrin receptor by perturbing the interaction between tyrosine motifs and the medium chain subunit of the AP-2 adaptor complex. *J Biol Chem* 278:12022–12028.
25. Dhonukshe P, et al. (2007) Clathrin-mediated constitutive endocytosis of PIN auxin efflux carriers in Arabidopsis. *Curr Biol* 17:520–527.
26. Takano J, Miwa K, Yuan L, von Wirén N, Fujiwara T (2005) Endocytosis and degradation of BOR1, a boron transporter of Arabidopsis thaliana, regulated by boron availability. *Proc Natl Acad Sci USA* 102:12276–12281.
27. Tamura K, et al. (2003) Why green fluorescent fusion proteins have not been observed in the vacuoles of higher plants. *Plant J* 35:545–555.
28. Ozkaynak E, Finley D, Varshavsky A (1984) The yeast ubiquitin gene: Head-to-tail repeats encoding a polyubiquitin precursor protein. *Nature* 312:663–666.
29. Lin CH, MacGurn JA, Chu T, Stefan CJ, Emr SD (2008) Arrestin-related ubiquitin-ligase adaptors regulate endocytosis and protein turnover at the cell surface. *Cell* 135: 714–725.
30. Rogers EE, Eide DJ, Guerinot ML (2000) Altered selectivity in an Arabidopsis metal transporter. *Proc Natl Acad Sci USA* 97:12356–12360.
31. Vert G, Briat JF, Curie C (2001) Arabidopsis IRT2 gene encodes a root-periphery iron transporter. *Plant J* 26:181–189.
32. Zimeri AM, Dhankher OP, McCaig B, Meagher RB (2005) The plant MT1 metallothioneins are stabilized by binding cadmiums and are required for cadmium tolerance and accumulation. *Plant Mol Biol* 58:839–855.
33. Galan JM, Haguenauer-Tsapis R (1997) Ubiquitin lys63 is involved in ubiquitination of a yeast plasma membrane protein. *EMBO J* 16:5847–5854.
34. Liu Y, Chang A (2006) Quality control of a mutant plasma membrane ATPase: Ubiquitylation prevents cell-surface stability. *J Cell Sci* 119:360–369.
35. Shenoy SK, Lefkowitz RJ (2005) Receptor-specific ubiquitination of beta-arrestin directs assembly and targeting of seven-transmembrane receptor signalosomes. *J Biol Chem* 280:15315–15324.
36. Bonifacino JS, Traub LM (2003) Signals for sorting of transmembrane proteins to endosomes and lysosomes. *Annu Rev Biochem* 72:395–447.
37. Meusser B, Hirsch C, Jarosch E, Sommer T (2005) ERAD: The long road to destruction. *Nat Cell Biol* 7:766–772.
38. Eide D, Broderius M, Fett J, Guerinot ML (1996) A novel iron-regulated metal transporter from plants identified by functional expression in yeast. *Proc Natl Acad Sci USA* 93:5624–5628.
39. Cadwell K, Coscoy L (2005) Ubiquitination on nonlysine residues by a viral E3 ubiquitin ligase. *Science* 309:127–130.
40. Wang X, et al. (2007) Ubiquitination of serine, threonine, or lysine residues on the cytoplasmic tail can induce ERAD of MHC-I by viral E3 ligase mK3. *J Cell Biol* 177: 613–624.
41. Helliwell SB, Losko S, Kaiser CA (2001) Components of a ubiquitin ligase complex specify polyubiquitination and intracellular trafficking of the general amino acid permease. *J Cell Biol* 153:649–662.
42. Longva KE, et al. (2002) Ubiquitination and proteasomal activity is required for transport of the EGF receptor to inner membranes of multivesicular bodies. *J Cell Biol* 156:843–854.
43. Raiborg C, Rusten TE, Stenmark H (2003) Protein sorting into multivesicular endosomes. *Curr Opin Cell Biol* 15:446–455.
44. van Kerkhof P, et al. (2001) Proteasome inhibitors block a late step in lysosomal transport of selected membrane but not soluble proteins. *Mol Biol Cell* 12:2556–2566.
45. Blondel MO, et al. (2004) Direct sorting of the yeast uracil permease to the endosomal system is controlled by uracil binding and Rsp5p-dependent ubiquitylation. *Mol Biol Cell* 15:883–895.
46. Geldner N, Hyman DL, Wang X, Schumacher K, Chory J (2007) Endosomal signaling of plant steroid receptor kinase BRI1. *Genes Dev* 21:1598–1602.
47. Robatzek S, Chinchilla D, Boller T (2006) Ligand-induced endocytosis of the pattern recognition receptor FLS2 in Arabidopsis. *Genes Dev* 20:537–542.
48. Arnaud N, et al. (2007) The iron-responsive element (IRE)/iron-regulatory protein 1 (IRP1)-cytosolic aconitase iron-regulatory switch does not operate in plants. *Biochem J* 405:523–531.
49. Santoni V, Vinh J, Pflieger D, Sommerer N, Maurel C (2003) A proteomic study reveals novel insights into the diversity of aquaporin forms expressed in the plasma membrane of plant roots. *Biochem J* 373:289–296.
50. Sauer M, Paciorek T, Benková E, Friml J (2006) Immunocytochemical techniques for whole-mount in situ protein localization in plants. *Nat Protoc* 1:98–103.